Improved LEO PNT Accuracy Enabled by Long Baseline Ephemeris Corrections

Joe Saroufim, Samer Hayek, Sharbel Kozhaya, and Zaher M. Kassas
The Ohio State University

BIOGRAPHY

Joe Saroufim is a Ph.D student in the Department of Electrical and Computer Engineering at The Ohio State University and a member of the Autonomous Systems Perception, Intelligence, and Navigation (ASPIN) Laboratory. He received a B.E. in Mechanical Engineering from the Lebanese American University. His current research interests include low Earth orbit satellites, situational awareness, autonomous vehicles, and sensor fusion.

Samer Hayek is a Ph.D student in the Department of Electrical and Computer Engineering at The Ohio State University and a member of the ASPIN Laboratory. He received a B.E. in Mechanical Engineering from the Lebanese American University. His current research interests include low Earth orbit satellites, autonomous vehicles, sensor fusion, and simultaneous localization and mapping.

Sharbel Kozhaya is a Ph.D student in the Department of Electrical and Computer Engineering at The Ohio State University and a member of the ASPIN Laboratory. He received a B.E. in Electrical Engineering from the Lebanese American University. His current research interests include opportunistic navigation, low Earth orbit satellites, cognitive software-defined radio, and 5G. He is the recipient of the 2023 IEEE/ION Position, Location, and Navigation Symposium (PLANS) best student paper award.

Zaher (Zak) M. Kassas is the TRC Endowed Chair in Intelligent Transportation Systems and a professor at The Ohio State University. He is the Director of the ASPIN Laboratory. He is also Director of the U.S. Department of Transportation Center: CARMEN (Center for Automated Vehicle Research with Multimodal AssurEd Navigation), focusing on navigation resiliency and security of highly automated transportation systems. He received a B.E. with Honors in Electrical Engineering from the Lebanese American University, an M.S. in Electrical and Computer Engineering from The Ohio State University, and an M.S.E. in Aerospace Engineering and a Ph.D. in Electrical and Computer Engineering from The University of Texas at Austin. He is a recipient of the National Science Foundation (NSF) CAREER award, Office of Naval Research (ONR) Young Investigator Program (YIP) award, Air Force Office of Scientific Research (AFOSR) YIP award, IEEE Walter Fried Award, IEEE Harry Rowe Mimno Award, Institute of Navigation (ION) Samuel Burka Award, and ION Col. Thomas Thurlow Award. He is a Fellow of the IEEE, a Fellow of the ION, and a Distinguished Lecturer of the IEEE Aerospace and Electronic Systems Society and the IEEE Intelligent Transportations Systems Society. His research interests include cyber-physical systems, navigation systems, low Earth orbit satellites, cognitive sensing, and intelligent transportation systems.

ABSTRACT

A model for the time-varying ephemeris error impact on low Earth orbit (LEO) satellites ranging measurements is derived and parameterized in terms of two parameters. It is shown that for a particular space vehicle (SV) location along the orbit, the ephemeris error has no impact on the extracted pseudorange measurements. This enables the disambiguation of timing and ephemeris errors at a stationary reference receiver. The two parameters can be estimated by the reference and communicated asynchronously to an unknown receiver listening to the same LEO SVs to correct for ephemeris ranging errors, leading to improved positioning, navigation, and timing (PNT) accuracy. A simulation study is presented to evaluate the efficacy of the correction approach. The study considered an unmanned aerial vehicle (UAV) traveling a 30.5 km trajectory in 600 seconds in Columbus, Ohio, USA, without global navigation satellite system (GNSS) signals. The UAV was assumed to be equipped with a tactical-grade inertial measurement unit (IMU), an altimeter, and a LEO receiver. Starting with an initial estimate of its own states from a GNSS receiver, the UAV navigated by fusing altimeter measurements in a loosely coupled fashion via an extended Kalman filter (EKF) to aid the onboard IMU, while LEO observables from 2 Orbcomm, 1 Iridium NEXT, 22 OneWeb, and 100 Starlink SVs were fused to aid the IMU in a tightly-coupled fashion. Four LEO-aided IMU navigation frameworks are compared: (i) using erroneous LEO ephemerides from simplified general perturbations (SGP4), initialized with two-line element (TLE); (ii) using corrected ephemerides, after receiving the two parameters from the reference receiver; (iii) using erroneous ephemerides from TLE+SGP4 along with differential measurements from the reference receiver; and (iv) using corrected ephemerides, after receiving the two parameters, along with differential measurements from the reference receiver. Assuming the reference receiver was placed in Columbus at a mean baseline distance of 13.9 km from the UAV, the three-dimensional (3-D) position root-mean squared error (RMSE) by the four frameworks was 477 m, 7.12 m, 8.39 m, and 1.51 m, respectively. Next, the UAV was simulated to navigate in Baltimore, Maryland, USA, at a mean baseline distance of 577 km from the reference receiver. Here,

Preprint of the 2024 ION GNSS+ Conference
Baltimore, Maryland, September 16–20, 2024

two frameworks were compared: (i) using all visible LEO SVs over Baltimore, regardless of their visibility over Columbus, with LEO ephemerides obtained from TLE+SGP4 and (ii) using only LEO SVs over Baltimore whose ephemerides were corrected by the reference receiver in Columbus. The 3-D position RMSE of the two frameworks were 490 m and 17.9 m, respectively, demonstrating the applicability of the proposed approach over long baselines.

I. INTRODUCTION

The rapid boom in broadband communication low Earth orbit (LEO) satellite constellations, called megaconstellations (e.g. Starlink, OneWeb, and Kuiper), led to a worldwide research interest to study LEO positioning, navigation, and timing (PNT) (Kassas et al., 2019; Psiaki, 2021; Hartnett, 2022; Celikbilek et al., 2022; Prol et al., 2022; Ye et al., 2023; Kassas et al., 2023; Khalife and Kassas, 2023; Dureppagari et al., 2023; Farhangian and Landry, 2023; Fan et al., 2024; Liu et al., 2024; Kang et al., 2024; Stock et al., 2024). Large investments within the space industry have also been made to develop LEO PNT systems by Iridium STL, Xona, and the European Space Agency (ESA) (Cobb et al., 2017; Reid et al., 2020; Ries et al., 2023).

LEO PNT approaches can be categorized into three classes: (i) *PNT-dedicated LEO* constellations aiming to offer global and precise PNT services (Egea-Roca et al., 2022; Ferre et al., 2022; Menzione and Paonni, 2023; Prol et al., 2024); (ii) *dual-purposed LEO* satellites to provide PNT services alongside their existing services (Iannucci and Humphreys, 2020; Nardin et al., 2021; Cassel et al., 2022; Wang et al., 2022); and (iii) *opportunistic LEO PNT* satellites exploiting non-PNT LEO signals to extract navigation observables including Doppler, pseudorange, and carrier phase (Huang et al., 2022; Zhao et al., 2022; Singh et al., 2022; Khalife et al., 2022). This paper focuses on the latter class.

Signals from LEO space vehicles (SVs) hold attractive PNT characteristics, compared to global navigation satellite system (GNSS) SVs in medium Earth orbit (MEO). First, the sheer number of LEO SVs covering the Earth with diverse prograde (e.g. Starlink, Orbcomm, and Globalstar) and retrograde (e.g. OneWeb and Iridium) orbits offers favorable position dilution of precision (PDOP) (Morales and Lohan, 2021). Second, with a relatively short orbital period of 1.5–2 hours, LEO SVs provide highly informative Doppler measurements, leading to improved PNT accuracy. Third, LEO megaconstellations transmit in higher frequency bands, making their signal less susceptible to ionospheric effects.

Nevertheless, opportunistically exploiting non-cooperative LEO SVs for PNT necessitates addressing three main challenges: (i) unknown signal properties, (ii) ambiguous SV and receiver clock errors, and (iii) inaccurate SV ephemerides. The first challenge has been tackled in recent literature by developing specialized receivers that, either estimate encoded signal parameters to generate navigation observables (Khalife and Kassas, 2019; Humphreys et al., 2023), or blindly estimate transmitted signals with no prior knowledge of their properties (i.e., via cognitive software-defined radio) (Kozhaya and Kassas, 2022; Kozhaya et al., 2023). This paper tackles the last two challenges.

Unlinke GNSS, most LEO SVs do not openly transmit navigation data with orbital elements and clock error corrections in their downlink signals. An estimate of the SVs' ephemerides can be obtained from two-line element (TLE) files, published and updated by the North American Aerospace Defense Command (NORAD). The TLE file can be used to compute an estimate of a satellite's ephemeris, which in turn initializes orbit propagation algorithms, including two-body, two-body with $J2$, simplified general perturbation 4 (SGP4) (Vallado and Crawford, 2008), etc. Nevertheless, each of these orbital elements suffers from certain uncertainty, leading to accumulated propagated ephemeris error, which may range from couple hundred meters to few kilometers, depending on the SV's position along the orbit and the period of propagation (Vetter, 2007; Khairallah and Kassas, 2021). The ephemeris error and the clock ambiguity map conjointly into an accumulated bias in extracted range-type measurements, leading to an erroneous PNT solution.

Methods to address the ephemeris error challenge in the literature can be classified into four categories: (i) closed-loop tracking (Khairallah and Kassas, 2021, 2024; Hayek et al., 2024); (ii) machine-learning orbit determination (Zhang et al., 2024; Caldas and Soares, 2024; Kassas et al., 2024a); (iii) LEO-augmented GNSS (Li et al., 2022; Menzione et al., 2023; Li et al., 2024); and (iv) differential navigation (Zhao et al., 2023; Saroufim et al., 2023b; Ji et al., 2023). Nevertheless, each of these methods suffers from certain limitations. First, for closed-loop tracking, the cross-track and radial position errors are less observable than the along-track error. Second, machine-learning techniques require large training data, in addition to the knowledge of ground truth ephemeris. Third, LEO-augmented GNSS requires the installation of GNSS receivers onboard LEO SVs. Finally, differential navigation requires time synchronization and a relatively short baseline between the reference receiver and navigating receiver.

A recent study provided a characterization of the along-track ephemeris error and its impact on non-differential and differential ranging measurements (Saroufim et al., 2023a, 2024). This paper builds on this study and makes the following contributions. First, a model for the time-varying ephemeris error impact on the ranging error is derived. Second, a spatiotemporal error disambiguation method is introduced to correct erroneous LEO SVs' ranging measurements. The corrections are communicated asynchronously in terms of two ephemeris parameters, estimated by a reference receiver to a navigating receiver at a long baseline, leading to improved PNT accuracy. Third, a simulation study is presented to evaluate the efficacy of the correction approach. The study considers an unmanned aerial vehicle (UAV) traveling a 30.5 km trajectory in 600 seconds in Columbus, Ohio,

USA, without GNSS signals. The UAV is assumed to be equipped with a tactical-grade inertial measurement unit (IMU), an altimeter, and a LEO receiver. Starting with an initial estimate of its own states from a GNSS receiver, the UAV navigates by fusing altimeter measurements in a loosely coupled fashion via an extended Kalman filter (EKF) to aid the onboard IMU, while LEO observables from 2 Orbcomm, 1 Iridium NEXT, 22 OneWeb, and 100 Starlink SVs were fused to aid the IMU in a tightly-coupled fashion. Four LEO-aided IMU navigation frameworks are compared: (i) using erroneous LEO ephemerides from SGP4, initialized with TLE; (ii) using corrected ephemerides, after receiving the two parameters from the reference receiver; (iii) using erroneous ephemerides from TLE+SGP4 along with differential measurements from the reference receiver; and (iv) using corrected ephemerides, after receiving the two parameters from the reference receiver, along with differential measurements from the reference receiver. Assuming the reference receiver was placed in Columbus at a mean baseline distance of 13.9 km from the UAV, the 3-D position root-mean squared error (RMSE) by the four frameworks was 477 m, 7.12 m, 8.39 m, and 1.51 m, respectively. Next, the UAV was simulated to navigate in Baltimore, Maryland, USA, at a mean baseline distance of 577 km from the reference receiver. Here, two frameworks were compared: (i) using all visible LEO SVs over Baltimore, regardless of their visibility over Columbus, with LEO ephemerides obtained from TLE+SGP4 and (ii) using only LEO SVs over Baltimore whose ephemerides were corrected by the reference receiver in Columbus. The 3-D position RMSE of the two frameworks were 490 m and 17.9 m, respectively, demonstrating the applicability of the proposed approach over long baselines.

The rest of the paper is organized as follows. Section II derives a model for the LEO SV range error due to a 3-D ephemeris error in terms of two unknown parameters. Section III presents a method to disambiguate spatiotemporal errors from the ranging error and estimate the two ephemeris parameters. Section IV presents a LEO-aided IMU navigation framework employing short baseline and long baseline ephemeris error corrections. Section V gives concluding remarks.

II. EPHEMERIS ERROR MAPPING INTO THE RANGE MEASUREMENT SPACE

This section derives analytical expressions mapping the error from the SV's state space (i.e., ephemeris error) to the measurement space (i.e., range). The resulting ranging error is parameterized in terms of two ephemeris parameters that will be exploited later to disambiguate the spatiotemporal errors.

Let $\{f\}$ represent the satellite's normal coordinate system NTW, referred to as the *Frenet* system, and explained in Figure 1 (Vallado, 2007). For non-cooperative LEO SVs, the true SV's position $\boldsymbol{r}_s$ and velocity $\boldsymbol{v}_s$ are unknown, but an "erroneous" estimate of the position $\hat{\boldsymbol{r}}_s$ and velocity $\hat{\boldsymbol{v}}_s$ can be obtained by propagating TLE data. During one SV passing, defined by the total time a LEO SV remains continuously visible at the receiver, the propagated error in the SV's ephemeris can be assumed to remain invariant in the NTW frame. Let $\boldsymbol{e}_r^f = [e_{r,N}, e_{r,T}, e_{r,W}]^\mathsf{T}$ denote the 3-D position error vector of the LEO satellite in the NTW frame, defined as

$$\boldsymbol{e}_r \triangleq \boldsymbol{r}_s(k) - \hat{\boldsymbol{r}}_s(k).$$

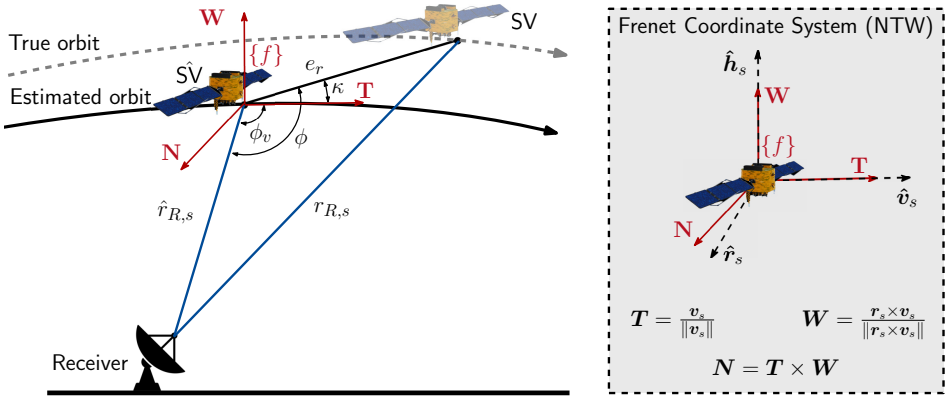

Figure 1: 3-D ephemeris error, e_r, and orientation, κ, in the NTW frame with the SV's true and estimated positions, and resulting ranges to the receiver.

Consider a stationary receiver R, with position vector $\boldsymbol{r}_R$, capable of extracting range-type measurements from an overhead LEO SV. With a sole access to TLE files, an error in the propagated ephemeris results in an erroneous range measurement $\hat{\boldsymbol{r}}_{R,s}$, with respect to the true range $\boldsymbol{r}_{R,s}$. The corresponding range error is defined as

$$\begin{aligned} \nu(k) &\triangleq \|\boldsymbol{r}_{R,s}(k)\| - \|\hat{\boldsymbol{r}}_{R,s}(k)\| \\ &= \|\boldsymbol{r}_R - \boldsymbol{r}_s(k')\| - \|\boldsymbol{r}_R - \hat{\boldsymbol{r}}_s(k')\|, \end{aligned} \tag{1}$$

where k' represents discrete-time instant $t_{k'} = kT + t_0 - \delta t_{\text{TOF}}$, with δt_{TOF} representing the true time-of-flight (TOF) of the signal from the LEO SV to the receiver. The paper will assume $k' \approx k$ to simplify the forthcoming derivation and the TOF error will be lumped into the dominating time and ephemeris errors. Following the analysis introduced in (Saroufim et al., 2024), the time-varying range error invoked by a 3-D ephemeris error $\boldsymbol{e}_r$ can be expressed as

$$\nu(k) = \hat{r}_{R,s}(k).\left[\left(1 - \frac{2.e_r.\cos\left(\phi_v(k) + \kappa\right)}{\hat{r}_{R,s}(k)}\right)^{\frac{1}{2}} - 1\right], \tag{2}$$

where $e_r \triangleq \|\boldsymbol{e}_r\|_2$, $\hat{r}_{R,s} \triangleq \|\hat{\boldsymbol{r}}_{R,s}\|_2$, and

$$\begin{aligned} \phi_v(k) &= \cos^{-1}\left(\frac{\langle \hat{\boldsymbol{v}}_s(k), \hat{\boldsymbol{r}}_{R,s}(k)\rangle}{\|\hat{\boldsymbol{v}}_s(k)\|.\|\hat{\boldsymbol{r}}_{R,s}(k)\|}\right) \\ \kappa &= \cos^{-1}\left(\frac{\langle \hat{\boldsymbol{v}}_s(k), \boldsymbol{e}_r\rangle}{\|\hat{\boldsymbol{v}}_s(k)\|.\|\boldsymbol{e}_r\|}\right). \end{aligned} \tag{3}$$

The ephemeris ranging error model in (2) is parameterized in terms of two unknown parameters, e_r and κ, fully characterizing the ephemeris error for each SV.

To analyze the effect of ephemeris errors on LEO SVs' ranging measurements, a simulation study was conducted using 650 Starlink LEO SVs. The latest TLE files of all SVs were parsed at the same time epoch, then propagated over a period of 270 minutes using two orbit determination algorithms: high precision orbit propagator (HPOP) and SGP4. A fixed receiver at The Ohio State University, Columbus, Ohio, was simulated to extract range-type measurements from all visible overhead LEO SVs with a minimum elevation of 10 degrees, as shown in Figure 2. Over the simulation period, the SGP4-propagated ephemeris, denoted by $\hat{\boldsymbol{r}}_s$ in this paper, accumulate errors with respect to the ground truth obtained by HPOP, and denoted $\boldsymbol{r}_s$.

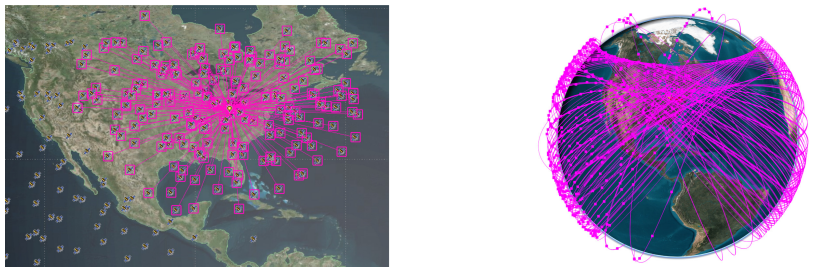

Figure 2: Locations of 650 simulated Starlink SVs over Columbus Ohio, USA (left) and their corresponding 3-D trajectories (right).

The resulting average position error and corresponding sample standard deviation over all 650 Starlink SVs are plotted in Figure 3. It can be seen that the error experiences two different behaviors: (i) it fluctuates during each orbital period depending on the SV position along its orbit, and (ii) it increases over time amongst different passings in all NTW components. It is important to note that the error is mainly concentrated in the in-track direction (T-axis), reaching almost 2 km after 4 hours of propagation, while attaining 200 m and 300 m for the radial and cross-track directions, respectively.

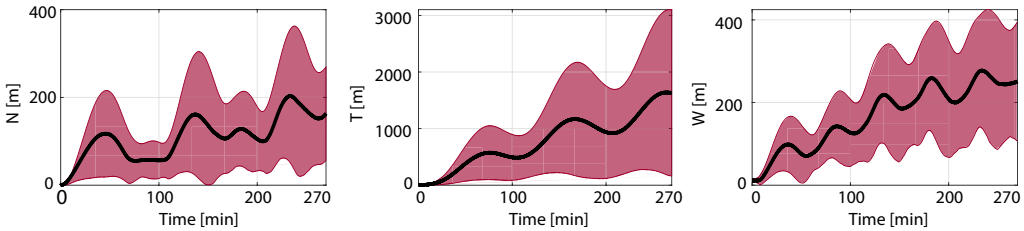

Figure 3: Average ephemeris position error and corresponding sample standard deviation in the NTW frame of the 650 Starlink SVs shown in Figure 2.

To demonstrate the validity of the proposed model, the analytical ephemeris ranging error obtained using (2) was compared to the empirical error given by (1) for 6 different Starlink SVs, along with their corresponding ephemeris parameters, e_r and κ. The results plotted in Figure 4 show that the proposed model accurately depicts the time-varying ephemeris ranging error given knowledge of the ephemeris parameters.

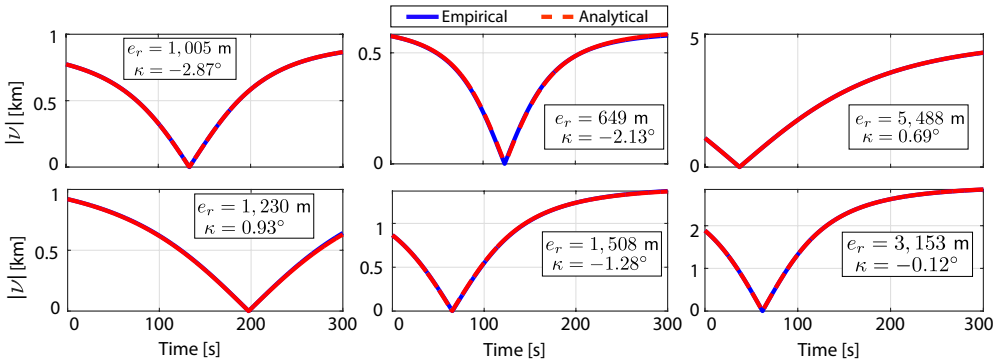

Figure 4: Empirical vs analytical ranging error due to accumulated ephemeris errors between SGP4 and HPOP for 6 Starlink LEO SVs, with their corresponding ephemeris parameters, e_r and κ.

III. DISAMBIGUATION OF SPATIOTEMPORAL ERRORS FROM LEO RANGING MEASUREMENTS

This section exploits the range error model in (2) to disambiguate the ephemeris error from the timing error in the extracted LEO SVs pseudorange measurements, and subsequently estimate the ephemeris parameters, e_r and κ, for each SV. These parameters will be used in the following section to correct the pseudorange measurements at an unknown receiver to achieve an accurate navigation solution.

Consider a stationary reference receiver with a known position $\boldsymbol{r}_{R_{\text{ref}}}$, extracting pseudorange measurements from a LEO satellite. The pseudorange ρ from the LEO SV to the receiver at time-step k is modeled as

$$\rho(k) = \|\boldsymbol{r}_{R_{\text{ref}}} - \boldsymbol{r}_s(k)\|_2 + c.\delta t^{(R_{\text{ref}},s)}(k) + c\delta t_{\text{trop}}(k) + c\delta t_{\text{iono}}(k) + \epsilon_\rho(k), \tag{4}$$

where $\delta t^{(R_{\text{ref}},s)}(k) \triangleq [\delta t_{R_{\text{ref}}}(k) - \delta t_s(k)]$ with $\delta t_{R_{\text{ref}}}$ and δt_s being the clock biases of the receiver and the LEO SV, respectively; c represents the speed-of-light; $\delta t_{\text{iono}}(k)$ and $\delta t_{\text{trop}}(k)$ are the ionospheric and tropospheric delays from the LEO SV to the receiver at time-step k, respectively; and ϵ_ρ is the pseudorange measurement noise, modeled as a discrete-time zero-mean white Gaussian sequence with variance $\sigma^2_\rho(k)$. Standard ionospheric and tropospheric estimation models (Misra and Enge, 2010; Sun et al., 2024) are assumed to be employed by the receiver to correct for the atmospheric delays; hence, $c\delta t_{\text{iono}}$ and $c\delta t_{\text{trop}}$ will be neglected in the forthcoming derivation. Define the function $f(t)$ as

$$\begin{aligned} f(t) &\triangleq \rho(t) - \|\boldsymbol{r}_{R_{\text{ref}}} - \hat{\boldsymbol{r}}_s(t)\| \\ &= \|\boldsymbol{r}_{R_{\text{ref}}} - \boldsymbol{r}_s(t)\| - \|\boldsymbol{r}_{R_{\text{ref}}} - \hat{\boldsymbol{r}}_s(t)\| + c.\delta t^{(R_{\text{ref}},s)}(t) \\ &= \nu(t) + c.\delta t^{(R_{\text{ref}},s)}(t), \end{aligned} \tag{5}$$

where in (5), a switch to continuous-time was adopted to simplify the analysis.

This paper will introduce a method aiming to disambiguate the spatiotemporal errors, namely $\nu(t)$ and $c.\delta t^{(R_{\text{ref}},s)}(t)$ from (5). For each SV, the corresponding function $f(t)$ has a unique inflection point, denoted $\{t^*, f(t^*)\}$, at which the ephemeris error term $\nu(t)$ vanishes and the value of $f(t)$ is equal to the clock bias, i.e., $f(t^*) = c.\delta t^{(R_{\text{ref}},s)}(t^*)$. Subsequently, it can be shown that $\phi(t^*) = \frac{\pi}{2}$ and hence the angle κ can be calculated as $\hat{\kappa} = \frac{\pi}{2} - \phi_v(t^*)$. Finally, the second ephemeris parameter, e_r, can be calculated at any point t_1 around t^* from (5) using the model in (1). Figure 5 shows the functions $f(t)$ and ephemeris ranging errors $\nu(t)$ for 4 different LEO SVs. The inflection point of $f(t)$ occurs at the zero-crossing of the corresponding ephemeris range error $\nu(t)$.

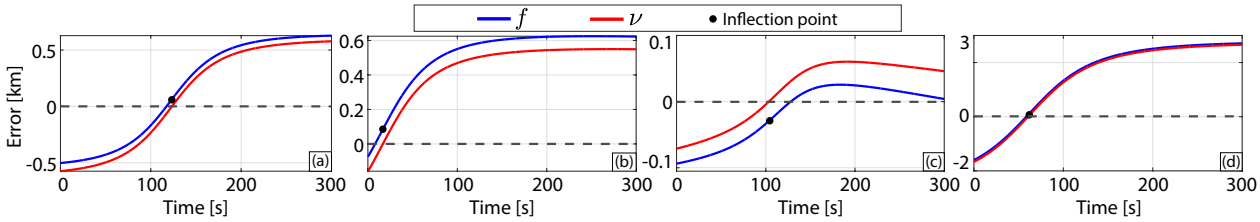

Figure 5: Range error function $f(t)$ and its inflection point corresponding to zero ephemeris ranging error for 4 different LEO SVs.

IV. LEO-AIDED IMU NAVIGATION WITH EPHEMERIS ERROR CORRECTION

This section presents a simulation study demonstrating the significance of disambiguating the LEO ephemeris and timing errors towards improving the accuracy of the navigation solution.

1. Simulation Description

The simulation considers a fixed reference receiver with known position, located at The Ohio State University, Columbus, Ohio, USA, extracting pseudorange measurements from overhead LEO SVs. This receiver estimates the ephemeris parameters described in Section III after disambiguating the spatiotemporal errors. These parameters are then communicated to a navigating fixed-wing UAV with an unknown position, $\boldsymbol{r}_R(k)$, to correct its pseudorange measurements from the same LEO SVs. The UAV is simulated to travel a distance of 30.5 km in 600 seconds without GNSS signals. The UAV was assumed to be equipped with a tactical grade IMU, an altimeter, and LEO receivers. Starting with an initial estimate of its own states from a GNSS receiver, the UAV navigated by fusing altimeter measurements in a loosely coupled fashion via an EKF with its onboard INS, while LEO observables from 2 Orbcomm, 1 Iridium NEXT, 22 OneWeb, and 100 Starlink SVs were fused to aid the INS in a tightly-coupled fashion. LEO SVs' ground truth trajectories were obtained by propagating TLE sets via HPOP, while the filter used SGP4-propagated ephemeris. Both orbit determination software were employed 4 hours prior to the simulation, where SGP4-propagated ephemeris accumulate error with respect to the ground truth generated via HPOP.

2. Case 1: UAV Navigation with Short Baseline Ephemeris Correction

The reference receiver was placed in Columbus, OH, at a mean baseline distance of 13.9 km from the UAV. Four navigation frameworks were compared:

- **Framework 1:** The UAV listens to all visible LEO SVs, and the filter uses erroneous SGP4 ephemeris. The EKF state vector is given by

$$\begin{aligned} \boldsymbol{x} &= \left[\boldsymbol{x}_R^\mathsf{T}, \boldsymbol{x}_{\text{clk}_1}^\mathsf{T}, \ldots, \boldsymbol{x}_{\text{clk}_L}^\mathsf{T}\right]^\mathsf{T} \in \mathbb{R}^{16+2L} \\ \boldsymbol{x}_R &= \left[{}^b_g\bar{\boldsymbol{q}}^\mathsf{T},\ \boldsymbol{r}_R^\mathsf{T},\ \dot{\boldsymbol{r}}_R^\mathsf{T},\ \boldsymbol{b}_{\text{gyr}}^\mathsf{T},\ \boldsymbol{b}_{\text{acc}}^\mathsf{T}\right]^\mathsf{T} \\ \boldsymbol{x}_{\text{clk}_j} &= \left[c\,\delta t^{(R,s_j)}, c\,\dot{\delta} t^{(R,s_j)}\right]^\mathsf{T}, \end{aligned}$$

  where L is the total number of satellites; $\boldsymbol{x}_R$ is the UAV's state vector, consisting of ${}^b_g\bar{\boldsymbol{q}}$, which is a 4-D unit quaternion vector characterizing the orientation of the IMU body frame $\{b\}$ with respect to the global frame $\{g\}$; $\boldsymbol{r}_R$ and $\dot{\boldsymbol{r}}_R$ represent the 3-D position and velocity of the UAV expressed in $\{g\}$; and $\boldsymbol{b}_{\text{gyr}}$ and $\boldsymbol{b}_{\text{acc}}$ are the 3-D biases of the gyroscope and accelerometer, respectively, expressed in $\{b\}$. The IMU equations used by the filter are explained in (Kassas et al., 2024b). The vector $\boldsymbol{x}_{\text{clk},l}$ is comprised of the difference between the UAV's and the j^{th} LEO SV's clock bias $c\,\delta t^{(R,s_j)}$ and drift $c\,\dot{\delta} t^{(R,s_j)}$.

- **Framework 2:** The UAV only listens to corrected LEO SVs, and the filter uses the estimated ephemeris parameters, e_r and κ, communicated by the reference receiver. The EKF state vector is the same as in framework 1, and the framework is explained in Figure 6. Note that each pair of parameters is communicated once to the navigating vehicle and used to estimate the time-varying ephemeris ranging error.

- **Framework 3:** The reference receiver also acts like a differential base station which communicates its measurements, position, and measurement noise statistics to the unknown UAV. The latter differences its measurements with those of the base station; hence, eliminating common mode errors between the two receivers (Saroufim et al., 2023b). The filter uses erroneous SGP4 ephemeris. The EKF state vector is given by

$$\begin{aligned} \boldsymbol{x} &= \left[\boldsymbol{x}_R^\mathsf{T}, \boldsymbol{x}_{\text{clk}}^\mathsf{T}\right]^\mathsf{T} \in \mathbb{R}^{18} \\ \boldsymbol{x}_{\text{clk}} &= \left[c\,\delta t^{(R_{\text{ref}},R)}, c\,\dot{\delta} t^{(R_{\text{ref}},R)}\right]^\mathsf{T}, \end{aligned}$$

  where $c\,\delta t^{(R_{\text{ref}},R)}$ and $c\,\dot{\delta} t^{(R_{\text{ref}},R)}$ represent the relative clock bias and drift between the unknown and reference receivers, respectively.

- **Framework 4:** Two types of corrections were applied: (i) differential corrections eliminating common mode errors similar to framework 3 and (ii) ephemeris corrections via the communicated ephemeris parameters similar to framework 2. The EKF state vector is the same as in framework 3.

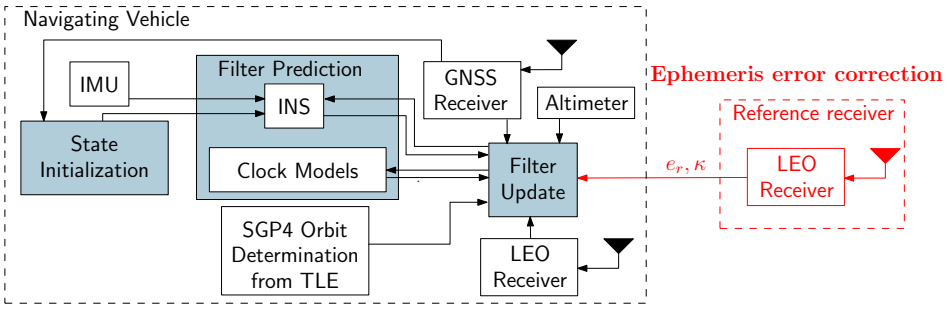

Figure 6: LEO-aided IMU navigation framework with ephemeris error corrections from a stationary reference receiver.

Figure 7 shows the EKF error plots of the UAV's position and velocity in the East-North-Up (ENU) reference frame for Framework 1 (columns 1 and 2) and Framework 2 (columns 3 and 4) along with the corresponding 3σ error bounds. It can be seen that relying on the erroneous SGP4 ephemeris (Framework 1) causes inconsistency in the EKF, and hence results in large positioning errors, namely a 3-D position RMSE of 477 m and a final error of 180 m. Nevertheless, correcting the estimated measurements by incorporating the ephemeris parameters communicated by the reference receiver yields consistency in the EKF, and significant error reduction to 7.12 m in position RMSE and 4.1 m in final error. On the other hand, Figure 8 shows the EKF error plots of the UAV's position and velocity in the ENU reference frame for Framework 3 (columns 1 and 2) and Framework 4 (columns 3 and 4) along with the corresponding 3σ error bounds. Although the EKF in Framework 3 is inconsistent in bounding the 3-D position errors induced by the erroneous SGP4 ephemeris, differential measurements significantly reduced the errors induced by the erroneous ephemerides, resulting in a position RMSE of 8.39 m and a final error of 10.3 m. Moreover, incorporating differential corrections along with the communicated ephemeris parameters leads to a consistent filter and a significant error reduction in position RMSE and final error to 1.51 m and 1.4 m, respectively. Table 1 summarizes the simulation results.

Table 1: Simulation Results

	Framework 1	**Framework 2**	**Framework 3**	**Framework 4**
3-D position RMSE [m]	477	7.12	8.39	1.51
Final error [m]	180	4.1	10.3	1.4

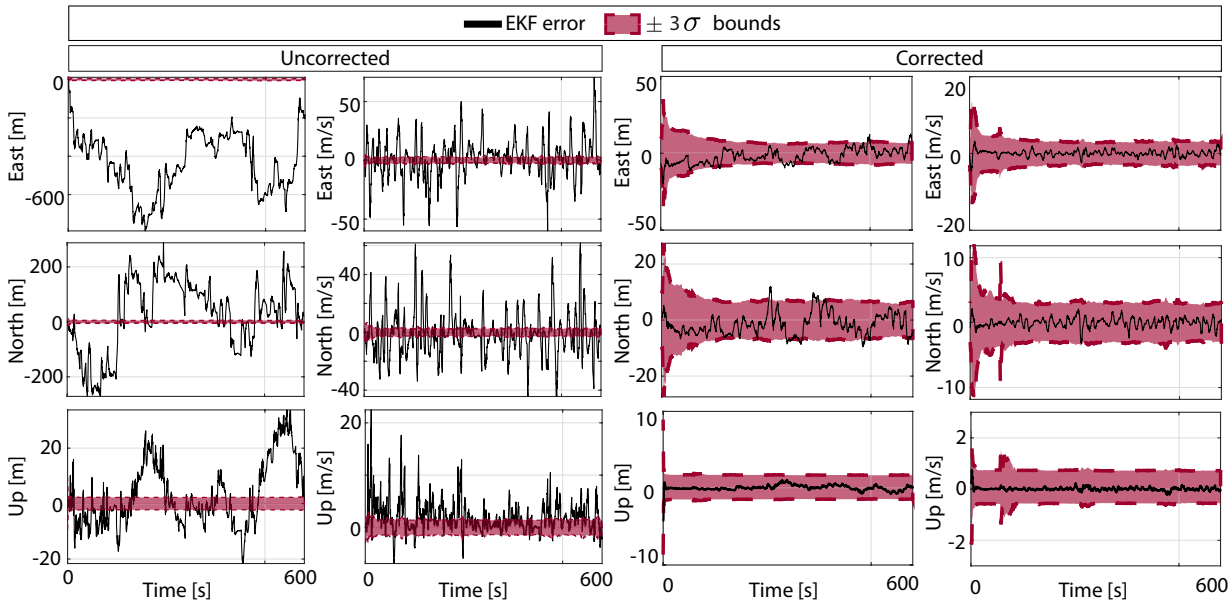

Figure 7: EKF estimation error plots of the UAV states with the $\pm 3\sigma$ bounds for Framework 1 (columns 1 and 2) and Framework 2 (columns 3 and 4). The first and second columns of each pair correspond to the position and velocity states, respectively, of the UAV in the ENU frame.

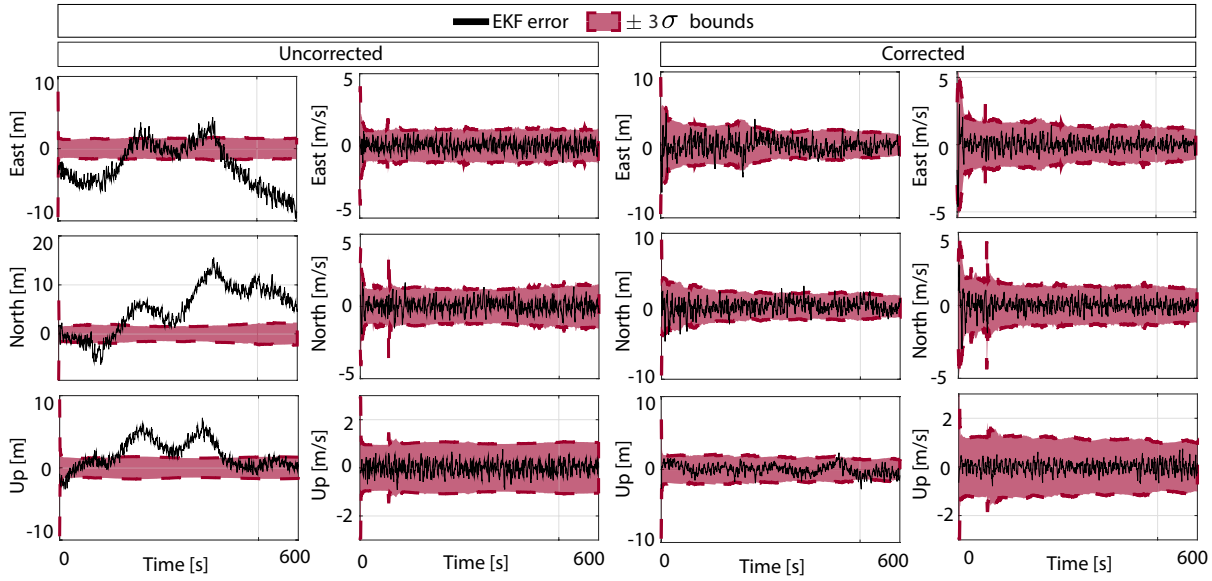

Figure 8: EKF estimation error plots of the UAV states with the $\pm 3\sigma$ bounds for Framework 3 (columns 1 and 2) and Framework 4 (columns 3 and 4). The first and second columns of each pair correspond to the position and velocity states, respectively, of the UAV in the ENU frame.

3. Case 2: UAV Navigation with Long Baseline Ephemeris Correction

In this subsection, the same UAV described above was simulated to navigate the same trajectory in Baltimore, Maryland, USA, while keeping the reference receiver at Columbus, Ohio, USA. The new mean baseline distance is 557 km, exceeding the operating range of differential as the errors at both receivers become highly uncorrelated. Note that some LEO SVs might not be simultaneously visible at both receivers, making the use of differential impractical. Therefore, this study considered the following frameworks:

- **Framework 1:** The UAV listens to all visible LEO SVs over Baltimore, Maryland, regardless of their visibility over Columbus, Ohio, and the filter uses erroneous SGP4 ephemeris. Here, the reference receiver is not used.
- **Framework 2:** The UAV only listens to the LEO SVs corrected by the reference receiver. The latter communicates the two ephemeris parameters of each SV to the UAV to correct its pseudorange measurements from SGP4.

Figure 9 shows the LEO SVs' trajectories, the reference receiver location, the UAV's ground truth trajectory, as well as the estimated trajectories via Framework 1 (uncorrected) and Framework 2 (corrected). Framework 1, incorporating erroneous ephemeris, resulted in a 3-D position RMSE of 490 m and a final error of 191 m, while Framework 2 achieved a position RMSE and final error of 17.9 m and 14.4 m, respectively. Although the corrections are communicated over a 557 km baseline, they accurately estimated the range error caused by the SGP4 ephemerides. The degradation in the navigation performance with respect to Framework 2 from Case 1 is due to the slight change in the SGP4-propagated error by the time the SVs reached Baltimore. Table 2 summarizes the simulation results.

Table 2: Simulation Results: Long Baseline Correction

	Framework 1	**Framework 2**
3-D position RMSE [m]	490	17.9
Final error [m]	191	14.4

V. CONCLUSION

This paper presented a theoretical model for the time-varying ephemeris error impact on the extracted LEO SV ranging measurements in terms of two unknown parameters. The model was then exploited to disambiguate the timing end ephemeris error terms from the ranging error at a stationary reference receiver. The reference receiver asynchronously communicate the two estimated parameters to a navigating receiver to correct its pseudorange measurements. Simulation results were presented demonstrating the efficacy of the proposed approach over long baseline.

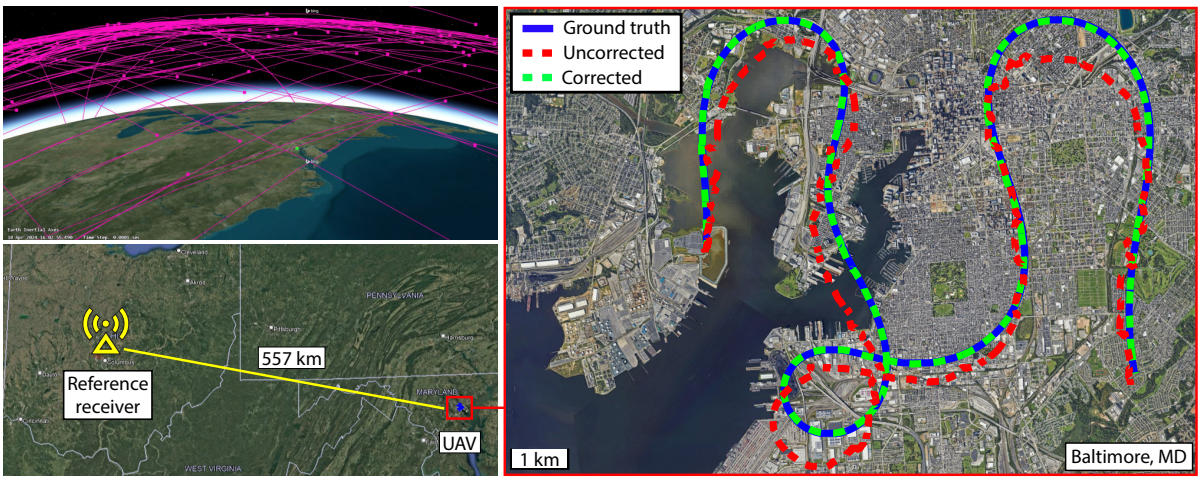

Figure 9: Simulation results showing the reference receiver location in Ohio, the aerial vehicle's trajectory in Maryland, estimated trajectories using uncorrected (scenario 1) and corrected (scenario 2) pseudorange measurements, and LEO SVs trajectories used in the simulation.

ACKNOWLEDGEMENTS

This work was supported in part by the Air Force Office of Scientific Research (AFOSR) under Grant FA9550-22-1-0476, the National Science Foundation (NSF) under Grant 2240512, and the U.S. Department of Transportation under Grant 69A3552348327 for the CARMEN+ University Transportation Center.

REFERENCES

Caldas, F. and Soares, C. (2024). Precise and efficient orbit prediction in LEO with machine learning using exogenous variables. In *Proceedings of IEEE Congress on Evolutionary Computation*, pages 1–8.

Cassel, R., Scherer, D., Wilburne, D., Hirschauer, J., and Burke, J. (2022). Impact of improved oscillator stability on LEO-based satellite navigation. In *Proceedings of ION International Technical Meeting*, pages 893–905.

Celikbilek, K., Saleem, Z., Morales Ferre, R., Praks, J., and Lohan, E. (2022). Survey on optimization methods for LEO-satellite-based networks with applications in future autonomous transportation. *Sensors*, 22(4):1–52.

Cobb, S., Lawrence, D., Gutt, G., and OConnor, M. (2017). Differential and rubidium disciplined test results from an Iridium-based secure timing solution. In *Proceedings of ION International Technical Meeting Conference*, pages 1111–1116.

Dureppagari, H., Saha, C., Dhillon, H., and Buehrer, R. (2023). NTN-based 6G localization: Vision, role of LEOs, and open problems. *IEEE Wireless Communications*, 30(6):44–51.

Egea-Roca, D., Lopez-Salcedo, J., Seco-Granados, G., and Falletti, E. (2022). Performance analysis of a multi-slope chirp spread spectrum signal for PNT in a LEO constellation. In *Proceedings of Workshop on Satellite Navigation Technology*, pages 1–9.

Fan, G., Chen, X., Zhang, R., Wu, P., Wei, Q., Xu, W., Dai, J., and Cao, L. (2024). Toward massive satellite signals of opportunity positioning: Challenges, methods and experiments. *Space: Science & Technology*, pages 1–21.

Farhangian, F. and Landry, R. (2023). High-order pseudorange rate measurement model for multi-constellation LEO/INS integration: Case of Iridium-NEXT, Orbcomm, and Globalstar. *Proceedings of the Institution of Mechanical Engineers, Part G: Journal of Aerospace Engineering*, 237(4):925–939.

Ferre, R., Praks, J., Seco-Granados, G., and Lohan, E. (2022). A feasibility study for signal-in-space design for leo-pnt solutions with miniaturized satellites. *IEEE Journal on Miniaturization for Air and Space Systems*, 3(4):171–183.

Hartnett, M. (2022). Performance assessment of navigation using carrier Doppler measurements from multiple LEO constellations. Master's thesis, Air Force Institute of Technology, Ohio, USA.

Hayek, S., Saroufim, J., and Kassas, Z. (2024). Ephemeris error correction for tracking non-cooperative LEO satellites with pseudorange measurements. In *Proceedings of IEEE Aerospace Conference*, pages 1–9.

Huang, C., Qin, H., Zhao, C., and Liang, H. (2022). Phase - time method: Accurate Doppler measurement for Iridium NEXT signals. *IEEE Transactions on Aerospace and Electronic Systems*, 58(6):5954–5962.

Humphreys, T., Iannucci, P., Komodromos, Z., and Graff, A. (2023). Signal structure of the Starlink Ku-band downlink. *IEEE Transactions on Aerospace and Electronics Systems*, 59(5):6016–6030.

Iannucci, P. and Humphreys, T. (2020). Economical fused LEO GNSS. In *Proceedings of IEEE/ION Position, Location and Navigation Symposium*, pages 426–443.

Ji, M., Luo, R., Xu, N., Li, Y., and Chen, X. (2023). An opportunistic LEO-based Doppler differential positioning method with baseline optimization. In *Proceedings of International Conference on Communication Network and Machine Learning*, pages 123–128.

Kang, J., Eberechukwu N, P., Lee, J., Wymeersch, H., and Kim, S. S. (2024). Fundamental performance bounds for carrier phase positioning in LEO-PNT systems. In *Proceedings of IEEE International Conference on Acoustics, Speech and Signal Processing*, pages 13496–13500.

Kassas, Z., Hayek, S., and Haidar-Ahmad, J. (2024a). LEO satellite orbit prediction via closed-loop machine learning with application to opportunistic navigation. *IEEE Aerospace and Electronic Systems Magazine*. accepted.

Kassas, Z., Khairallah, N., and Kozhaya, S. (2024b). Ad astra: Simultaneous tracking and navigation with megaconstellation LEO satellites. *IEEE Aerospace and Electronic Systems Magazine*, 39(9):46–71.

Kassas, Z., Kozhaya, S., Kanj, H., Saroufim, J., Hayek, S., Neinavaie, M., Khairallah, N., and Khalife, J. (2023). Navigation with multi-constellation LEO satellite signals of opportunity: Starlink, Oneweb, Orbcomm, and Iridium. In *Proceedings of IEEE/ION Position, Location, and Navigation Symposium*, pages 338–343.

Kassas, Z., Morales, J., and Khalife, J. (2019). New-age satellite-based navigation – STAN: simultaneous tracking and navigation with LEO satellite signals. *Inside GNSS Magazine*, 14(4):56–65.

Khairallah, N. and Kassas, Z. (2021). Ephemeris closed-loop tracking of LEO satellites with pseudorange and Doppler measurements. In *Proceedings of ION GNSS Conference*, pages 2544–2555.

Khairallah, N. and Kassas, Z. (2024). Ephemeris tracking and error propagation analysis of LEO satellites with application to opportunistic navigation. *IEEE Transactions on Aerospace and Electronic Systems*, 60(2):1242–1259.

Khalife, J. and Kassas, Z. (2019). Receiver design for Doppler positioning with LEO satellites. In *Proceedings of IEEE International Conference on Acoustics, Speech and Signal Processing*, pages 5506–5510.

Khalife, J. and Kassas, Z. (2023). Performance-driven design of carrier phase differential navigation frameworks with mega-constellation LEO satellites. *IEEE Transactions on Aerospace and Electronic Systems*, 59(3):2947–2966.

Khalife, J., Neinavaie, M., and Kassas, Z. (2022). The first carrier phase tracking and positioning results with Starlink LEO satellite signals. *IEEE Transactions on Aerospace and Electronic Systems*, 56(2):1487–1491.

Kozhaya, S., Kanj, H., and Kassas, Z. (2023). Multi-constellation blind beacon estimation, Doppler tracking, and opportunistic positioning with OneWeb, Starlink, Iridium NEXT, and Orbcomm LEO satellites. In *Proceedings of IEEE/ION Position, Location, and Navigation Symposium*, pages 1184–1195.

Kozhaya, S. and Kassas, Z. (2022). Blind receiver for LEO beacon estimation with application to UAV carrier phase differential navigation. In *Proceedings of ION GNSS Conference*, pages 2385–2397.

Li, M., Xu, T., Guan, M., Gao, F., and Jiang, N. (2022). LEO-constellation-augmented multi-GNSS real-time PPP for rapid re-convergence in harsh environments. *GPS Solutions*, 26(1):1–12.

Li, X., Yuan, Y., Han, X., Li, X., and Fu, Y. (2024). Toward wide-area and high-precision positioning with LEO constellation augmented PPP-RTK. *IEEE Transactions on Instrumentation and Measurement*, 73:1–13.

Liu, P., Voon Ling, K., Qin, H., Jiang, M., and Lu, J. (2024). Actualization analysis of LEO opportunistic doppler aided GNSS precise point positioning using moving horizon estimation. *IEEE Transactions on Vehicular Technology*, pages 1–12. accepted.

Menzione, F. and Paonni, M. (2023). LEO-PNT mega-constellations: a new design driver for the next generation MEO GNSS space service volume and spaceborne receivers. In *Proceedings of IEEE/ION Position, Location, and Navigation Symposium*, pages 1196–1207.

Menzione, F., Renga, A., and Santoro, G. (2023). Configurable GNSS based orbit determination for LEO-PNT non-operative and operative phases. In *Proceedings of IEEE International Workshop on Metrology for AeroSpace*, pages 603–608.

Misra, P. and Enge, P. (2010). *Global Positioning System: Signals, Measurements, and Performance*. Ganga-Jamuna Press, second edition.

Morales, R. and Lohan, E. (2021). Comparison of MEO, LEO, and terrestrial IoT configurations in terms of GDOP and achievable positioning accuracies. *IEEE Journal of Radio Frequency Identification*, 5(3):287–299.

Nardin, A., Dovis, F., and Fraire, J. (2021). Empowering the tracking performance of LEO-based positioning by means of meta-signals. *IEEE Journal of Radio Frequency Identification*, 5(3):244–253.

Prol, F., Bhuiyan, M., Kaasalainen, S., Lohan, S., Praks, J., Celikbilek, K., and Kuusniemi, H. (2024). Simulations of dedicated LEO-PNT systems for precise point positioning: Methodology, parameter analysis, and accuracy evaluation. *IEEE Transactions on Aerospace and Electronic Systems*, pages 1–19. accepted.

Prol, F., Ferre, R., Saleem, Z., Välisuo, P., Pinell, C., Lohan, E., Elsanhoury, M., Elmusrati, M., Islam, S., Celikbilek, K., Selvan, K., Yliaho, J., Rutledge, K., Ojala, A., Ferranti, L., Praks, J., Bhuiyan, M., Kaasalainen, S., and Kuusniemi, H. (2022). Position, navigation, and timing (PNT) through low earth orbit (LEO) satellites: A survey on current status, challenges, and opportunities. *IEEE Access*, 10:83971–84002.

Psiaki, M. (2021). Navigation using carrier Doppler shift from a LEO constellation: TRANSIT on steroids. *NAVIGATION, Journal of the Institute of Navigation*, 68(3):621–641.

Reid, T., Chan, B., Goel, A., Gunning, K., Manning, B., Martin, J., Neish, A., Perkins, A., and Tarantino, P. (2020). Satellite navigation for the age of autonomy. In *Proceedings of IEEE/ION Position, Location and Navigation Symposium*, pages 342–352.

Ries, L., Limon, M., Grec, F., Anghileri, M., Prieto-Cerdeira, R., Abel, F., Miguez, J., Perello-Gisbert, J., d'Addio, S., R. Ioannidis and, A. O., Rapisarda, M., Sarnadas, R., and Testani, P. (2023). LEO-PNT for augmenting Europe's space-based PNT capabilities. In *Proceedings of IEEE/ION Position, Location, and Navigation Symposium*, pages 329–337.

Saroufim, J., Hayek, S., and Kassas, Z. (2023a). Evaluation of orbit errors and measurement corrections in differential navigation with LEO satellites. In *Proceedings of ION GNSS+ Conference*, pages 2823–2834.

Saroufim, J., Hayek, S., and Kassas, Z. (2023b). Simultaneous LEO satellite tracking and differential LEO-aided IMU navigation. In *Proceedings of IEEE/ION Position Location and Navigation Symposium*, pages 179–188.

Saroufim, J., Hayek, S., and Kassas, Z. (2024). Analysis of satellite ephemeris error in differential and non-differential navigation with LEO satellites. In *Proceedings of IEEE Aerospace Conference*, pages 1–9.

Singh, U., Shankar, M., and Ottersten, B. (2022). Opportunistic localization using LEO signals. In *Proceedings of Asilomar Conference on Signals, Systems, and Computers*, pages 894–899.

Stock, W., Schwarz, R., Hofmann, C., and Knopp, A. (2024). Survey on opportunistic PNT with signals from LEO communication satellites. *IEEE Communications Surveys & Tutorials*, pages 1–31. accepted.

Sun, A., Morton, Y., and Lee, J. (2024). Ionospheric scintillation effects across multiple carrier frequency bands transmitted from LEO satellites. In *Proceedings of ION International Technical Meeting*, pages 109–125.

Vallado, D. (2007). *Fundamentals of Astrodynamics and Applications*. Springer, third edition.

Vallado, D. and Crawford, P. (2008). SGP4 orbit determination. In *Proceedings of AIAA/AAS Astrodynamics Specialist Conference and Exhibit*, pages 6770–6799.

Vetter, J. (2007). Fifty years of orbit determination: Development of modern astrodynamics methods. *Johns Hopkins APL Technical Digest*, 27(3):239–252.

Wang, M., Liu, G., Ma, R., Zhao, W., and Kang, W. (2022). A novel navigation-communication integrated waveform for LEO network. In *Proceedings of IEEE Global Communications Conference*, pages 747–752.

Ye, L., Gao, N., Yang, Y., Deng, L., and Li, H. (2023). Three satellites dynamic switching range integrated navigation and positioning algorithm with clock bias cancellation and altimeter assistance. *Aerospace*, 10(5):411–438.

Zhang, W., Zhang, K., Li, X., Wu, J., Yuan, Y., and Fu, Y. (2024). A novel method for improving LEO kinematic real-time precise orbit determination with neural networks. *IEEE Transactions on Instrumentation and Measurement*, 73:1–12.

Zhao, C., Qin, H., and Li, Z. (2022). Doppler measurements from multiconstellations in opportunistic navigation. *IEEE Transactions on Instrumentation and Measurement*, 71:1–9.

Zhao, C., Qin, H., Wu, N., and Wang, D. (2023). Analysis of baseline impact on differential Doppler positioning and performance improvement method for LEO opportunistic navigation. *IEEE Transactions on Instrumentation and Measurement*, 72:1–10.